

The Metastable Dynamo Model of Stellar Rotational Evolution

Timothy M. Brown

Las Cumbres Observatory Global Telescope Network, 6740 Cortona Dr. Suite 102, Goleta, CA 93117, USA; tbrown@lcogt.net

ABSTRACT

This paper introduces a new empirical model for the rotational evolution of Sun-like stars – those with surface convection zones and non-convective interior regions. Previous models do not match the morphology of observed (rotation period)-color diagrams, notably the existence of a relatively long-lived “C-sequence” of fast rotators first identified by Barnes (2003). This failure motivates the Metastable Dynamo Model (MDM) described here. The MDM posits that stars are born with their magnetic dynamos operating in a mode that couples very weakly to the stellar wind, so their (initially very short) rotation periods at first change little with time. At some point, this mode spontaneously and randomly changes to a strongly-coupled mode, the transition occurring with a mass-dependent lifetime that is of order 100 MYr. I show that with this assumption, one can obtain good fits to observations of young clusters, particularly for ages of 150 MYr to 200 MYr. Previous models and the MDM both give qualitative agreement with the morphology of the slower-rotating “I-sequence” stars, but none of them accurately reproduce the stellar-mass-dependent evolution of the I-sequence stars, for clusters older than a few hundred MYr. I discuss observational experiments that can test aspects of the MDM, and speculate that the physics underlying the MDM may be related to other situations described in the literature, in which stellar dynamos may have a multi-modal character.

Keywords: stars: rotation – stars: activity – stars: magnetic field – stars: solar-type

1. Stellar Rotation: Phenomenology and Theory

In recent years, improved observational methods have drawn attention to subtle features of stars, notably the rotational period, and the strength and character of stellar magnetic activity. Observational progress has been particularly marked in relation to stellar rotation, and to the asymmetric surface structures (magnetic in origin) that are its visible symptoms.

Rotational periods can be measured accurately by observing the brightness modulation as spotted stars spin.

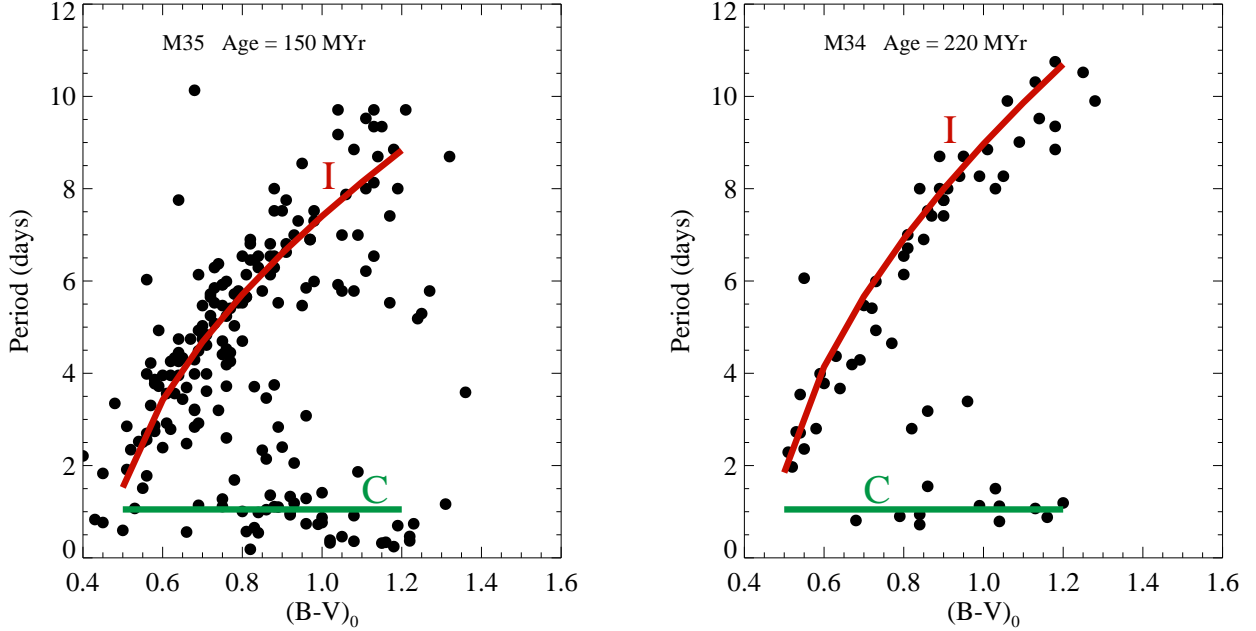


Fig. 1.— Rotational period P_{rot} plotted against dereddened $(B - V)$ color, for the intermediate-age clusters M35 (left) and M34 (right). Most stars lie on one of two principal sequences, identified as C and I by Barnes (2003), although some stars are found in the intervening gap. Data are from Meibom et al. (2009, 2011a).

Figure 1 shows such rotation periods P_{rot} (days), plotted against dereddened $(B - V)$ color for stars in the clusters M35 (Meibom et al. 2009), age about 150 MYr, and M34 (Meibom et al. 2011b), age about 220 MYr. The stars plotted here (and considered in the rest of this paper) are all Sun-like, in the sense that they have vigorous surface convection zones (CZs), with radiative zones underneath. Thus, these stars span spectral types from mid-F to early-M. The P_{rot} data plotted in this Figure come from period analysis of the brightness modulation of rotating spotted stars. The stars with measurements are therefore those that display evidence of asymmetrically distributed starspots. Moreover, the stars represented in the Figure have been carefully vetted, using radial velocity data and other criteria, to reject non-members of the respective clusters. The question naturally arises whether these visibly-spotted stars, which typically comprise about half of the cluster stars observed, are representative of the cluster population. Fortunately, spectroscopic observations of cluster stars with and without starspot modulation indicate that there are no systematic differences between these two groups (Jackson & Jeffries 2012).

Of primary interest in the Figure are two relatively tight sequences of stars (labeled *I* and *C*, after Barnes (2003)). The *I*-sequence consists of relatively slow rotators. With increasing age t , the *I*-sequence becomes more tightly defined, and moves to longer periods (roughly $P_{rot} \propto t^{1/2}$), as the outflow of magnetized stellar winds drain angular momentum from the stars. Stars on the *C*-sequence are rapid rotators. In young clusters $t \leq 150$ MYr, the *C*-sequence has members that span the mass range of Sun-like stars. In older clusters the *C*-sequence erodes away, starting with the higher-mass stars. By the age of the Hyades (600 MYr), the only remaining fast rotators are M-type dwarfs. Between the sequences (the “gap”), the P_{rot} -color diagram shows a paucity of stars, but it is by no means empty.

Since the 1980s, considerable theoretical work has gone into modeling the processes leading to the behavior illustrated in Fig. 1. In the next section I will outline the conceptual basis for three such models, one of which, the Metastable Dynamo Model (MDM), is described here for the first time. All of these incorporate magnetic wind braking to slow stellar rotation with age, but they differ in respect to other processes that may be acting within stars.

2. Current Models and Their Fit to Observations

2.1. 2-Zone Model

The prevailing model of the evolution of stellar rotation is what I term here the 2-Zone Model (2ZM). It has evolved over the last 25 years from the stellar wind torque law in the form written by Kawaler (1988), with still earlier progenitors including Weber & Davis (1967); Mestel (1968) and Belcher & MacGregor (1976). Since the early 1990s, the model has been extended and tested against successively improved observations in a series of papers, e.g. Pinsonneault et al. (1990); MacGregor & Brenner (1991); Krishnamurthi et al. (1997); Irwin & Bouvier (2009); Denissenkov et al. (2010); Epstein & Pinsonneault (2014). Stripped of most physical justification, the model may be summarized as follows:

(1) The torque acting on a star because of its magnetized stellar wind is given by the bifurcated expression

$$\begin{aligned} \frac{dJ}{dt} &= K_W \Omega^3 \left[\frac{R}{M} \right]^{1/2}, & \Omega \leq \Omega_{crit}, \\ &= K_W \Omega \Omega_{crit}^2 \left[\frac{R}{M} \right]^{1/2}, & \Omega \geq \Omega_{crit}, \end{aligned} \quad (1)$$

where J is the star’s total angular momentum, M and R are the star’s mass and radius (both in solar units), and Ω is the stellar rotation frequency, usually expressed in units of the Sun’s

rotation frequency of about 3×10^{-6} rad s $^{-1}$. The constant K_W has the dimensions of a moment of inertia (g cm 2) and is chosen to give the solar rotation frequency at the solar age. This expression (with torque scaling as Ω^3 for slow rotators) yields the Skumanich (1972) $t^{-1/2}$ rotation law for old stars.

(2) Initial conditions are applied at an age of 1 to 20 MYr counting from the birth line of Palla & Stahler (1990), corresponding to current estimates of the time during which contracting protostars are magnetically locked to their natal disks. Initial rotation periods P_0 are usually in the range 1 to 15 days, corresponding to the period distributions seen in the youngest open clusters (e.g., Rebull (2001); Rebull et al. (2004)).

(3) The dynamo saturation frequency Ω_{crit} is actually taken to be a function of stellar mass M_* (or equivalently of $(B - V)$ color). Its effect in the model is to decrease the torque acting on fast-rotating (periods of a few days or less) stars, so their short rotation periods can survive long enough for us to see them in clusters with ages as great as 500 MYr.

(4) The angular momentum in stellar convection zones is assumed to be weakly coupled to that in their radiative interiors. This allows the CZ to rotate more or less independently of the star’s interior. The coupling is characterized by an equilibration timescale τ_c , which is a function of stellar mass, increasing from 10 MYr for stars with more than solar mass, to greater than 100 MYr for early M-type stars. In addition, to avoid spoiling the fit to fast-rotating stars, τ_c must depend also on Ω itself, being 1 MYr or less for rapid rotators, and attaining the values just mentioned only for slow rotators (Denissenkov et al. 2010). Thus τ_c is, in principle, a free function of mass and Ω . As a simplification, Denissenkov et al. (2010) took τ_c to be short (1 MYr) for stars rotating faster than a critical period P_{crit} ; otherwise τ_c was taken to be long, of order 100 MYr. In either case, the equilibrium rotation frequency of the CZ is determined by balancing the angular momentum flux across the bottom of the CZ with that lost to the stellar wind.

2.2. Barnes’s Symmetrical Empirical Model

Barnes (2010) and Barnes & Kim (2010) sought to describe observed cluster P_{rot} -color diagrams empirically, connecting their expressions with astrophysical concepts only after obtaining a satisfactory fit to the observations. For purposes of this paper, I call their model the Symmetrical Empirical Model (SEM). Its logic runs as follows:

- (1) Stars on the I - and C -sequences obey different period-evolution equations, namely

$$P_I(B - V, t) = f(B - V)g(t), \quad (I - \text{sequence}) \quad (2)$$

$$P_C(B - V, t) = P_0 e^{[t/T(B-V)]}. \quad (C - \text{sequence})$$

Here $g(t) = t^{-1/2}$, as in the Skumanich law, P_0 is a constant period, and the functions $f(B - V)$ and $T(B - V)$ are initially arbitrary functions that can be determined from fits to the observations. Both $T(B - V)$ and $f^2(B - V)$ have dimensions of time. Barnes & Kim (2010) note that both these functions appear to be related in simple ways to a physically interesting quantity, namely the turnover time of the convection zone, denoted τ .

(2) Accepting this identification, the period evolution expressions can be combined into one period evolution equation that has the correct behavior both for large and small values of the period P :

$$\frac{dP}{dt} = \left[\frac{k_I P}{\tau} + \frac{\tau}{k_C P} \right]^{-1}, \quad (3)$$

where k_I and k_C are dimensionless constants determined from fits to the data. This equation gives the SEM its name. To parallel the development of the 2ZM, I transform the period evolution equation to a torque law, assuming solid-body rotation, so that the relevant moment of inertias for both sequences are equal to the total stellar value I_* . The resulting torque law is

$$\frac{dJ}{dt} = -I_* \frac{\Omega^2}{2\pi} \left[\frac{2\pi k_I}{\tau \Omega} + \frac{\tau \Omega}{2\pi k_C} \right]^{-1}. \quad (4)$$

(3) Initial conditions may be applied as with the 2ZM, though Barnes (2010) prefers to set initial periods at the zero-age main sequence (ZAMS), roughly 50 MYr after the birth line. At this time the rotation periods are at their shortest, limited at the short-period end by the breakup equatorial speed of the star.

The SEM is a descriptive, not explanatory model, as Barnes & Kim (2010) take pains to point out. That is, the physical processes that determine the functions $f(B - V)$ and $T(B - V)$ are not specified. The possible connection between these functions and the convective turnover time τ is, however, suggestive. If the reality of this relationship can be verified, then it might place a useful constraint on more physics-based models of stellar magnetic fields.

3. Computing the Rotation Evolution with Time

Based on the prescriptions in the previous section, it is fairly straightforward to compute the time evolution of P_{rot} at the surface of a star, according to either the 2ZM or the SEM. In addition to the torque equations given above, for this purpose one requires the time history of the radii and moments of inertia of the stellar radiative zone and outer convective

envelope. I computed these quantities for a set of 11 models with initial masses of $\{0.3, 0.4, \dots, 1.3\} \times M_{\odot}$, using the MESA suite of stellar evolution codes (Paxton et al. 2011). These were standard (non-rotating) models using solar abundances and default settings for all microphysics processes. As discussed by, *e.g.*, Denissenkov et al. (2010), gross structural differences between rotating and non-rotating stars are small except for Ω near the break-up value, and are not of qualitative importance for the rotational evolution. For masses intermediate between the computed models, I obtained the needed radii and moments by linear interpolation between models. Because the MESA timesteps were not always small enough for stable numerical integrations of the rotation, I also interpolated the stellar data onto a finer time grid, typically involving 3000 time steps to span the Sun’s age, roughly equally spaced in $\log t$. For a direct comparison of my computed results with published ones, I computed $(B - V)$ and the convective turnover time τ from the tabular functions of mass (evaluated at an age of 500 MYr) given by Barnes & Kim (2010)). (τ is plotted in their Fig. 9.)

Lastly, one requires initial conditions, namely the interval τ_{disk} between the Palla & Stahler (1990) birth line and the time when the star unlocks from the protostellar disk, and $P0$, the star’s rotation period at unlocking. In the following simulations I set τ_{disk} to either 5 or 10 MYr, depending on which published results I sought to emulate. In all cases, I drew $P0$ values from a distribution intended to mimic (independent of stellar mass) the observed rotation periods in the Orion Nebula Cluster (ONC), as compiled in the Open Cluster Database (Mermilliod 1995), drawing data from Walker (1990); Eaton et al. (1995); Choi & Herbst (1996) and Rebull (2001). Fig. 2 shows this initial period distribution. It develops, however, that there is no qualitative difference between the population synthesis results for the ONC *vs.* a uniform distribution between $P0$ of 1 to 15 days, for cluster ages above about 100 MYr. As elaborated below, this is a result of the convergent nature of the Ω^3 torque law ascribed by all three model classes (2ZM, SEM, MDM) to stars of greater age. For population synthesis computations, I usually drew stellar masses from a uniform distribution spanning the range of masses in the MESA models. When attempting to match model parameters to specific cluster observations, however, I drew masses from distributions constructed to reproduce the observed number of stars *vs.* $(B - V)$ color.

4. Comparing the 2ZM and SEM to P_{rot} -color Diagrams

Fig. 3 shows the observed P_{rot} -color distribution for three open clusters of different ages (top row of panels), along with population synthesis models at the same nominal ages using the 2ZM (middle row) and SEM (bottom row). Both the 2ZM and SEM models are calibrated

to give the solar rotation period at the solar age, for a $1M_{\odot}$ star.

4.1. The 2ZM

For the 2ZM model results, I used parameter values within the bounds suggested by Denissenkov et al. (2010): $\tau_{disk} = 5$ MYr, $\Omega_{crit} = 8\Omega_{\odot}$, $P0_{crit} = 4$ days, and $\tau_c = 50$ MYr for $1 M_{\odot}$, increasing to 200 MYr for $0.5 M_{\odot}$. Denissenkov et al. (2010) did not offer a specific recipe for the functional form of $\tau_c(\text{mass})$; for definiteness, I made it proportional to the convective turnover time τ . For the ONC initial period distribution and $P0_{crit} = 4$ days, about half of the stars rotate as solid bodies, and half display differential rotation, with their convection zones decoupled from their interiors. In the Figure, the solid body rotators (henceforth SB) are shown in red, and the differential rotators (henceforth DR) in black.

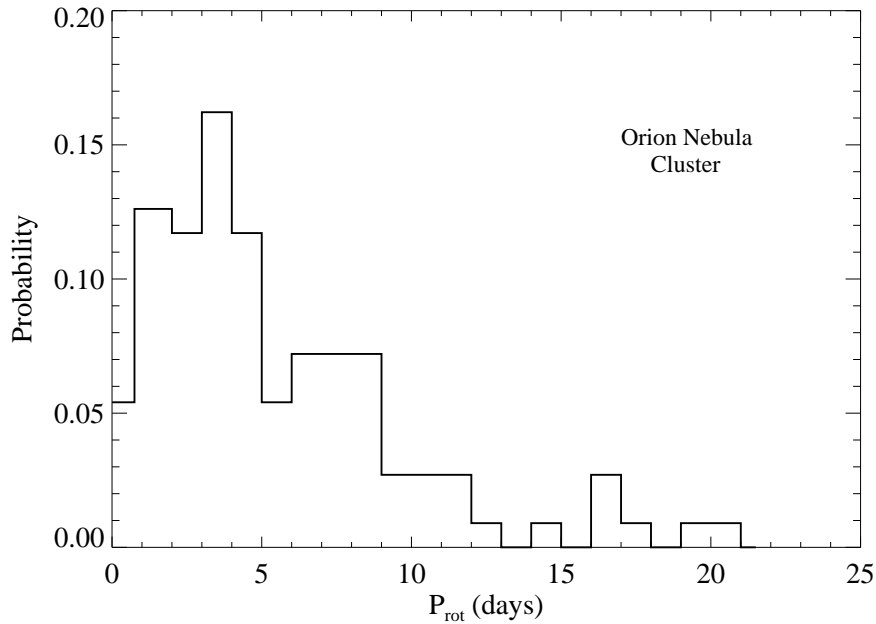


Fig. 2.— Initial period $P0$ probability distribution assumed for all population synthesis models in this paper. $P0$ is the rotation period that applies at the “birth line” of Palla & Stahler (1990), and also (by definition) the period at the end of the disk-locking time τ_{disk} for the particular star or model in question. This distribution is derived from the Open Cluster Database (Mermilliod 1995), with original data from Walker (1990); Eaton et al. (1995); Choi & Herbst (1996); Rebull (2001).

With suitable parameter choices, the 2ZM reproduces the top and bottom 10th percentile points of the surface rotation distributions in 16 open clusters of various ages (Denissenkov et al.

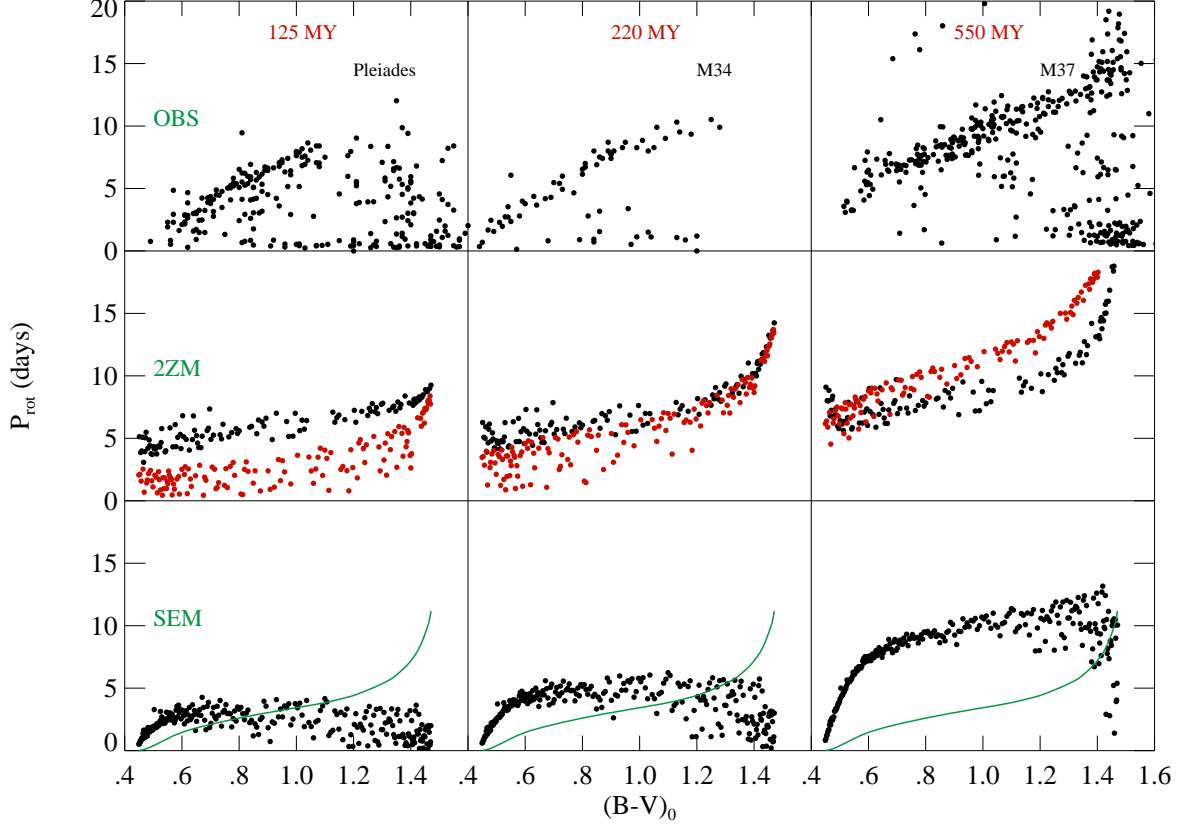


Fig. 3.— Comparison of observed (top row of panels) P_{rot} -color diagram for the open clusters {Pleiades, M34, M37} with the results of population synthesis for the 2ZM (middle row), and SEM (bottom row) models. Observations are from (Pleiades: Hartman et al. (2010)), (M34: Meibom et al. (2011a)), (M37: Hartman et al. (2009)). Both models are calibrated to give the solar rotation rate for a $1-M_{\odot}$ star at the solar age, and all start with 250 stars having $\tau_{disk} = 5$ MYr, initial periods distributed as in the Orion Nebula Cluster, and masses uniformly distributed over $0.4M_{\odot} \leq M \leq 1.2M_{\odot}$. The 2ZM parameters are in the ranges given by Denissenkov et al. (2010); red symbols indicate stars with initial periods P_0 so small that they rotate essentially as solid bodies, while black symbols denote stars with larger P_0 , so that their convection zones and radiative interiors may rotate at widely different rates. The SEM parameters agree with Barnes & Kim (2010); green curves show $P_{gap}(B - V)$, where period evolution is fastest. Detailed parameter values are given in the text.

2010). Note, however, that to get this agreement, both τ_{disk} and $P0$ must be large to match the slow rotators, and both must be small for the fast rotators. In the current population synthesis with $P0$ distributed in accord with observations of the ONC, the agreement with observed P_{rot} -color diagrams is not good. At 125 MYr, the SB and DR groups form two distinct sequences, with the SBs spinning faster. But the SBs move to longer periods faster than the DRs, so that by 220 MYr the gap between the sequences disappears, and the two sequences merge into one. Also by this age the true C-sequence stars (those with periods shorter than about 2 days) are found only at larger masses; none appear for masses below about $0.9 M_{\odot}$. This contradicts the observed behavior that rapid rotators disappear first at larger masses. At later ages dP_{rot}/dt for the SBs continues to be larger than for the DRs, so that by 550 MYr there are once again two sequences, but at this age the SBs have longer periods than the DRs, and neither group contains any stars with periods shorter than about 5 days.

The crossing behavior of the SB and DR sequences results from the smaller torque hypothesized to act on the members of the DR sequence, this torque being determined by angular momentum transport between the stellar interior and the envelope, rather than between the envelope and the wind. By disconnecting the interior from the wind torque, the differential rotation hypothesis allows models in which the surface rotation rate first decelerates quickly, and then stalls at a near-constant value for an extended time (e.g. Krishnamurthi et al. (1997); Denissenkov et al. (2010)). Meanwhile, the torque acting on the SB stars is larger than on the DRs of similar mass, typically by large factors. Thus, eventually the SBs spin down to periods that are longer than those of the DRs. For equal mass stars, this generates crossing paths in P_{rot} -age space, as shown in Fig. 4. The only evident way to avoid such crossings (and hence to preserve an age-independent I/C sequence morphology) is to consider groups of stars for which the SB/DR distinction necessarily entails large differences in $P0$ and/or τ_{disk} . (Fig. 8 of Denissenkov et al. (2010) shows such an example.) But in a population synthesis involving continuous distributions of $P0$ and τ_{disk} , such correlated behavior among the various initial values would require new rules in a model prescription that is already rather complicated. Alternatively, better agreement between observations and theory can likely be obtained by suitably tuning the distribution of $P0$, or through a different prescription for determining the strength of the core/envelope coupling. The range of such possibilities is wide, however, and investigating whether such modifications of the 2ZM might provide an acceptable representation of the data is beyond the scope of this paper. I therefore note only that the 2ZM parameters commonly found in the literature seem to lead to an unsatisfactory comparison with observations.

4.2. The SEM

By construction, the Symmetrical Empirical Model (Barnes 2010; Barnes & Kim 2010) attempts to match the high- and low- P_{rot} envelopes of observed clusters. But (given a set of initial periods) it also predicts the period distribution of stars in the gap between the C - and I -sequences. As noted by Barnes (2010), for each mass there is a period $P_{gap} = \tau / \sqrt{k_I k_C}$, for which dP/dt reaches a maximum. Using the computed mass dependence of τ and $(B - V)$, one can construct the curve in P_{rot} -color space along which this maximum occurs. This is shown as the green curve in the bottom row of panels of Fig. 3. Via a conventional evolution/population argument, one expects the density of stars along this curve to be smaller than at neighboring periods. Barnes (2010) suggests this as an observational test of the theory, and displays data from three clusters (the Pleiades, M35, and M37) that provide

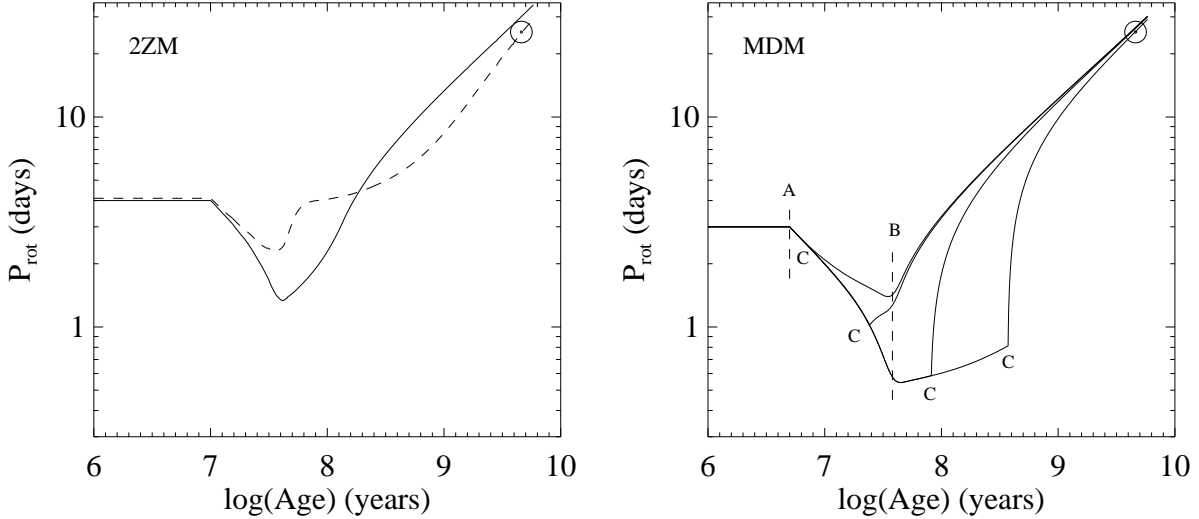


Fig. 4.— Left: Evolution of two models according to the 2ZM. Both models are for $1 M_{\odot}$ and identical initial rotation conditions P_0 and τ_{disk} . The solid curve shows solid body (SB) rotation, while the dashed curve shows the envelope P_{rot} for a model with radial differential (DR) rotation. The Sun symbol shows the solar age and P_{rot} values. Right: Rotational evolution for four MDM models. All correspond to $1 M_{\odot}$ and to $P_0 = 3$ days, $\tau_{disk} = 5$ MYr. The vertical dashed line **A** corresponds to disk unlocking, **B** to the star’s arrival on the main sequence, and the lines **C** to transitions from the weakly- to strongly-coupled dynamo modes occurring at $\{10, 30, 100, \text{ and } 300\}$ MYr (left to right). Note that in the strongly-coupled mode, angular momentum loss may be significant during the pre-main-sequence phase.

some support for the idea. Nonetheless, population synthesis carried out with the SEM, starting with the ONC period distribution, does not produce a clear C -sequence (Fig. 3, bottom row). Although dP_{rot}/dt is a maximum along the P_{gap} curve, the variation of dP_{rot}/dt with P_{rot} over the relevant range of periods is not very large. As a result the low density of stars along the P_{gap} curve is difficult to discern. Moreover the P_{gap} locus makes a clean boundary between the C - and I -sequences only for a limited range of cluster ages. It thus seems doubtful that the SEM’s period evolution structure is responsible for the existence of the C -sequence. The SEM I -sequence is well defined, especially at later ages, but overall the synthesized morphology in the P_{rot} -color diagram is not a good match to observations.

Once all the stars in a cluster have unlocked from their disks, the SEM preserves the ordering of stars in period for each mass. Thus, the lower envelope of the period distribution is determined by the minimum P_0 found at each mass, and dP_{rot}/dt scales inversely with $\tau(M_*)$. The effect is that rapidly-spinning stars evolve to periods longer than (say) 2 days at younger ages for high-mass stars than for low-mass ones (in qualitative agreement with observations). But the evolution rate is such that for intermediate masses (corresponding to $(B - V) \leq 1.2$ or so, all stars evolve to $P_{rot} \geq 2$ days within less than 200 MYr, even if P_0 is so large that their peak equatorial velocity reaches the centrifugal breakup speed. This leads to a total absence of stars in the SEM at short periods and moderate masses. There appears to be no way within the SEM to produce intermediate-mass stars with ages above 200 MYr and $P_{rot} \leq 2$ days, as are observed in M34 and M37. Moreover, the SEM gives a distribution of P_{rot} between its upper and lower envelopes that is more or less uniform at all masses. This does not resemble the observed distribution, in which the well-populated I and C -sequences are separated by a gap that is sparsely populated, but not empty.

As with the 2ZM, it is likely that one could improve the fit between the SEM and observations via appropriate adjustments of its parameters. But this too is outside the scope of the current discussion. Rather, in the next section I describe a different model that achieves the desired agreement more simply.

5. Metastable Dynamo Model

Here I introduce a third approach, which I call the Metastable Dynamo Model (MDM), and which offers a new way to understand the observed P_{rot} data. It derives from Barnes’s SEM, but in constructing the model, I have re-interpreted his function $T(B - V)$. The assumptions going into the MDM are:

- (1) Stars on the main sequence rotate as solid bodies, with little or no radial differential

rotation. Note that though the Sun rotates differentially in latitude, it is no exception to this rule; appropriately averaged over latitude, the Sun’s convection zone rotates (so far as helioseismology can show) at virtually the same rate as its radiative interior (Gilman et al. 1989; Tomczyk et al. 1995).

(2) Initial rotation conditions are given by conventional disk-locking processes, as for the 2ZM and SEM above.

(3) Stars spin down according to the torque law

$$dJ/dt = K_M \Omega^3 f^2(B - V), \quad (5)$$

where $f^2(B - V)$ is the same as in Barnes’s SEM model. As in the SEM, this function contains all of the mass dependence of the magnetized wind torque.

(4) The leading constant K_M may take one of two values, a “strong coupling” one (K_{M1}) that is consistent with a solar-mass star having the solar rotation period at the solar age, and a “weak coupling” one (K_{M0}) that is much smaller, perhaps by a factor of 100 or more. I tentatively identify these two values as manifestations of dynamo modes that are structured in different ways, perhaps like Barnes’s (2003) “Interface” and “Convective” dynamos. This notion gives the MDM its name, but for now is a conjecture.

(5) At the time that a star unlocks from its disk, it occupies the weak-coupling mode. It then spontaneously, randomly, and permanently flips to the strong-coupling mode. The transition probability for this flip per unit time is given by $1/\tau_M(M_*)$, which is essentially the reciprocal of Barnes’s function $T(B - V)$. This is to say, here I assume that $\tau_M(M_*)$ scales with the convective turnover time $\tau(M_*)$. The assumption that all stars start in the weak-coupling mode is arbitrary, and motivated largely by simplicity.

The time history of a star’s P_{rot} according to the MDM is not a deterministic function of its initial conditions; the random transition between coupling modes introduces a stochastic element into the evolution. Several possible tracks in P_{rot} -age space are illustrated in the right-hand panel of Fig. 4. These all correspond to identical initial conditions, but with varying ages for the transition between coupling modes. Observe that even for late transitions (e.g., at age ≥ 300 MYr), the period convergence caused by the Ω^3 torque law assures that all stars of a given mass arrive at the solar age with very similar rotational periods.

The MDM makes no use of the dynamo saturation frequency Ω_{crit} . This is not to suggest that magnetic saturation does not occur; there is strong evidence for such an effect on the X-ray emission from magnetically active stars, e.g. (Stauffer et al. 1994; Pizzolato et al. 2003). Rather, within the MDM framework, almost all stars that rotate faster than Ω_{crit} are ones that have not yet made the transition from the weak-coupling mode. For these stars, the

difference between Ω^3 and $\Omega\Omega_{crit}^2$ is negligible compared to the difference between K_{M0} and K_{M1} .

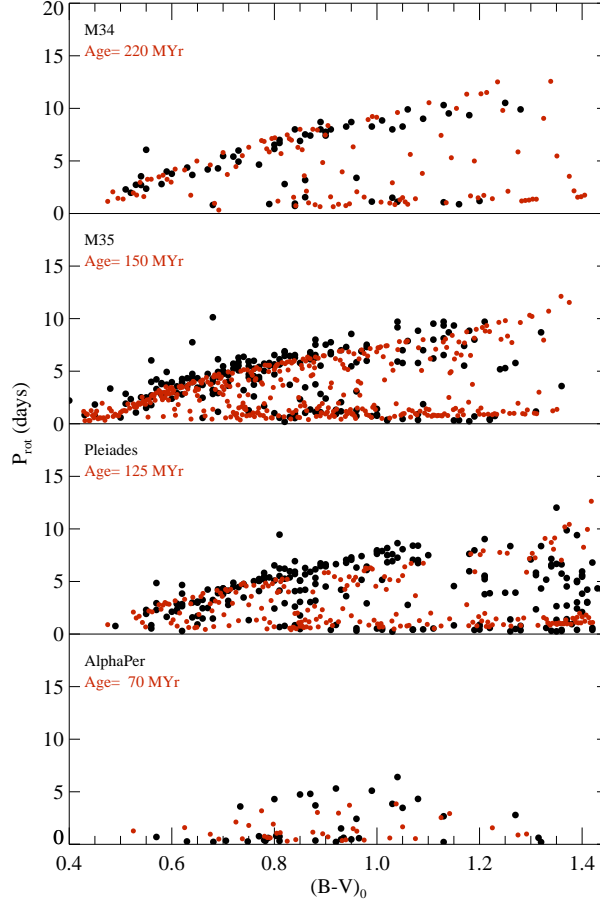


Fig. 5.— Overlaid observations (black dots) and MDM population synthesis simulations (red dots) for clusters α Per, Pleiades, M35, and M34, (from bottom to top), approximate ages 70, 125, 150, and 220 MYr, respectively. Observations are from (α Per: as tabulated in Mermilliod (1995)), (Pleiades: Hartman et al. (2010)), (M35: Meibom et al. (2009)), (M34: Meibom et al. (2011a)). The MDM model parameters are those found by maximizing the joint (over colors) Kolmogorov-Smirnov probability that model and observed distributions for M34 are drawn from the same distribution (*cf.* sections 6.1-6.2). Parameters used for these simulations were $\tau_{disk} = 5$ MYr, $K_{M0} = 5 \times 10^{29}$ g cm², $K_{M1} = 7 \times 10^{31}$ g cm², $\tau_M = 80$ MYr for stars of $1 M_{\odot}$, scaling as the convective turnover time τ . The function $f(B - V)$ defining the shape of the I -sequence is proportional to $\tau^{1/2}$, as in the SEM and Barnes & Kim (2010).

Figures 5 and 6 show comparisons between observations and MDM population synthesis models for eight clusters of various ages. For the simulations in these Figures, I constrained the number of model stars in bins of similar $(B - V)$ color (width 0.1 mag) to be equal to the number actually observed in the corresponding cluster. Otherwise, the simulations are strictly analogous to those in Fig. 3. Evidently the gross morphology of these simulations is much more like the observations than for the 2ZM and SEM models used in Fig. 3. The behavior of the observed C -sequence is captured by the models: there are many stars in it for

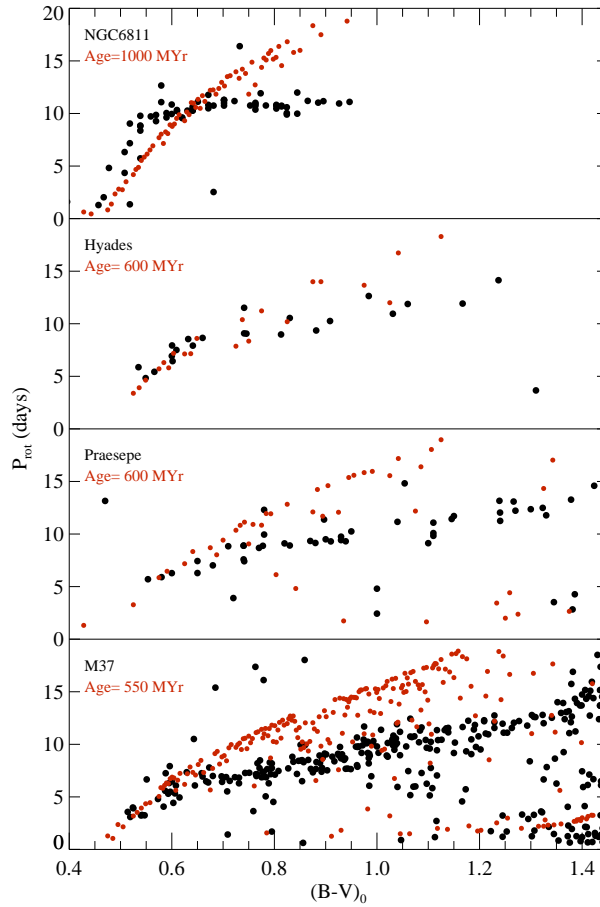


Fig. 6.— Same as Fig. 5, but for the older clusters (bottom to top) M37, Praesepe, Hyades, NGC 6811, with approximate ages 550, 600, 600, and 1000 MYr, respectively. Observations are from (M37: Hartman et al. (2009)), (Praesepe: Delorme et al. (2011)), (Hyades: as tabulated in the Open Cluster Database Mermilliod (1995)), NGC 6811: Meibom et al. (2011b)).

the younger clusters, but by the age of the Hyades there are few or none. Also the modeled C -sequence begins to thin out first at the higher masses, as it is observed to do. The most notable defect with respect to the C -sequence is that the models may overpopulate it at young ages. The comparison between observed and modeled I -sequences is best at around 200 MYr; the sequence’s slope and shape are slightly incorrect for the Pleiades, and much more so for the older clusters Hyades, Praesepe, and NGC 6811. Similar problems occur with the 2ZM and SEM models, however. All of the models act so that the shape of the I -sequence remains nearly constant in time, merely scaling in magnitude with age. The comparison shown here illustrates that this is too simple a description; more complicated physics will have to be invoked to explain the true I -sequence behavior.

Clearly the MDM is, like the SEM, a purely descriptive model. In common with the 2ZM and SEM, it implicitly invokes processes that have little or no quantitative physical basis (but see recent work on bistable dynamos, *e.g.* Morin et al. (2011); Gondoin (2012, 2013); Cook et al. (2013).) Nevertheless, the simulations show that, with plausible initial conditions, the MDM reproduces the appearance of observed P_{rot} -color diagrams fairly well. At a qualitative level, this is perhaps unsurprising. The strongly-coupled stars follow the same torque law as for the 2ZM and the SEM, hence must converge to a narrow I -sequence at large ages. Similarly, the model hypothesizes weakly-coupled stars precisely to create a relatively long-lived C -sequence of short-period rotators. The detailed shape $P_{rot}(M_*)$ of the I -sequence, as well as the number density of stars along the C -sequence as a function of age, both depend on free functions of mass that are poorly motivated by theory. Thus, the essential features of the MDM that distinguish it from the 2ZM and SEM are these: (1) Rapidly-rotating stars may for hundreds of MYr exist in a state in which they lose very little angular momentum. (2) When stars leave this weakly-coupled state, they quickly evolve to much longer P_{rot} . In other words, when it occurs, the transition in torque felt by the star must be large in magnitude and nearly discontinuous in time.

The qualitative success of the MDM is thought-provoking (though of course not conclusive in regard to physical origins). It suggests that the idea of metastable modes in stellar magnetic evolution may be a fruitful one. Fortunately, there are several observational tests that may be used to help validate or reject the model. I will discuss these in Section 7.2 below.

6. Quantitative Comparison of Rotation Models to Observations

6.1. Methodology

To better understand the successes and failures of the rotation evolution models, and to estimate the best parameter values for the MDM, it is useful to compute a quantitative measure of the goodness of fit of the models to the cluster rotation data. For this purpose, I used a Kolmogorov-Smirnov (K-S) procedure. For each model considered (2ZM, SEM, or MDM with various parameter values) and each of several $(B - V)$ color bins, I computed the period evolution for a cohort of 10^4 stars, uniformly distributed in mass so as to span the desired color bin, using the mass-color relation at 500 MYr age as tabulated by Barnes & Kim (2010), with P_0 values randomly drawn from the ONC distribution shown in Fig. 2. To simplify the computation, I ignored the evolution of $(B - V)$ with age. Moreover, I reduced the dimensionality of the problem by assuming a single disk-locking age $\tau_{disk} = 5$ MYr for all models. These evolutions started at the Palla & Stahler (1990) birth line, and ran to a maximum age of 6 GYr. For any desired age, I could then estimate the rotational probability distribution $\Phi_j(P_{rot}, [B - V]_j, t)$. Φ_j is normalized so that $\int \Phi_j dP_{rot} = 1$, separately for each color bin j and each age. Figure 7 illustrates such probability distributions for several $(B - V)$ values, estimated using the MDM for an age of 250 MYr.

The model Φ_j distributions in Fig. 7 are useful for illustrative purposes. But to compare the models to observations of a particular cluster a , it is simpler to lump each set of periods (modeled and observed) into bins according to $(B - V)$, and then use the two-sided Kolmogorov-Smirnov test (Press et al. 1989) to estimate for each color bin j the probability U_{aj} that the two period sets are drawn from the same distribution. To compare the success of various models in representing observations from a given cluster a , I used a figure of merit defined as $U_a = \Sigma_j \log_{10}(U_{aj})$. This choice corresponds to the \log_{10} of the probability that observations and simulations are drawn from the same distributions, jointly for all of the four color bins. Note that since the numerical value of U_a depends on the number of stars in the $(B - V)$ bins, this figure of merit may not be used to compare the representations of different clusters, even using the same model. For the results described below, I used four $(B - V)$ bins, with blue and red boundaries given by $\{(0.57, 0.66), (0.67, 0.81), (0.81, 1.01), (1.01, 1.21)\}$. From the 500 MYr mass-to-color relationship from Barnes & Kim (2010), this corresponds to masses of approximately $\{(1.1, 1.0), (0.99, 0.89), (0.89, 0.79), (0.79, 0.69)\} M_{\odot}$.

6.2. Optimum Parameters for MDM

Using the K-S measure of goodness-of-fit to the cluster rotation data, one can place limits on the parameters that appear in the MDM torque law. If the physical basis of the MDM is taken seriously, then such limits should constrain the processes whereby angular momentum is lost to the stellar wind, as well as the nature of the transition from weak to strong angular momentum coupling.

The purely theoretical torque law for strongly-coupled stars in the MDM is given in Eq.

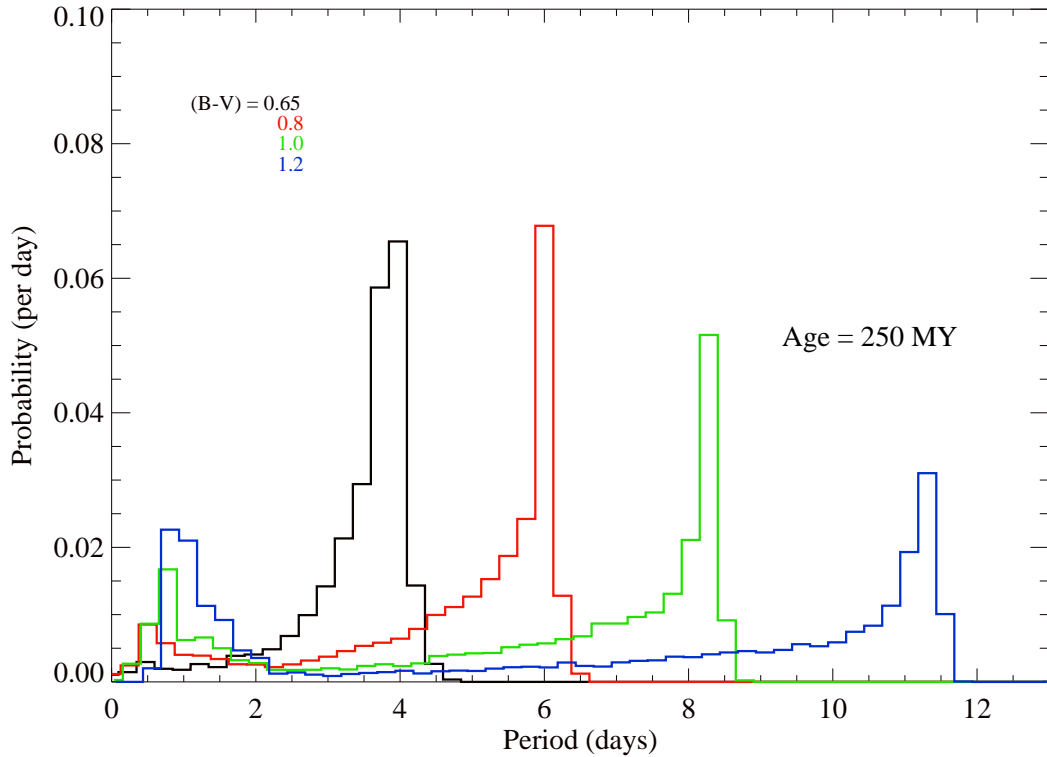


Fig. 7.— MDM-derived probability distributions for four $(B - V)$ colors, for stellar cohorts at an age of 250 MYr. At this age, the distributions are bimodal for all $(B - V)$ redder than about 0.65, with an increasingly large fraction of stars in the C -sequence (roughly $P_{rot} \leq 2$ days) as $(B - V)$ increases. Between the short- and long-period peaks, minima in the distributions are reached for P_{rot} between 1 and 3 days, depending on color. Stars with rotation periods near and just above these values have recently transitioned to the strong-coupling mode, and are evolving to longer periods at the maximum rate.

(5). In the discussion so far, I have assumed that the mass-dependent part of the torque is simply related to the star’s convective turnover time τ by $f^2(B-V) = 2\tau/k_I$ (Barnes & Kim 2010), and also that the constant K_{M1} is such as to give a $1-M_\odot$ star the solar rotation period at the solar age. There are thus only two free parameters in the pure form of the MDM: the weak-coupling constant K_{M0} and the transition timescale τ_M from the weakly- to the strongly-coupled modes.

The data do not place strong constraints on K_{M0} ; all that can be said is that it must be very small. To estimate a limit I computed the value of K_{M0} that degraded the fit for the 220-MYr cluster M34 so that the figure of merit U_a decreased by 1.3 relative to $K_{M0} = 0$ (corresponding to a 20-fold decrease in the probability that the observed and model period distributions were drawn from the same parent distribution). This procedure yields an upper limit of $K_{M0} \leq 2 \times 10^{30} \text{ g cm}^2$, about 350 times smaller than K_{M1} . Applying the same criterion $\delta U_a = -1.3$ yields limits to the transition timescale of $59 \text{ MYr} \leq \tau_M \leq 116 \text{ MYr}$, with the best-fit $\tau_M = 80 \text{ MYr}$.

Using Barnes’s (Barnes & Kim 2010) relation between the convective turnover time τ and $f^2(B-V)$, and the solar-rotation-consistent value for K_{M1} (with individually optimized K_{M0} and τ_M) yields a poor fit to the M34 data ($U_{M34} = -13.65$). To learn whether plausible variations in the torque law might give a significantly better fit, I generalized the strong-coupling MDM torque law as follows:

$$\frac{dJ}{dt} = SK_{M1} [f^2(B-V)]^{1+\gamma} \Omega^3, \quad (6)$$

where the exponent γ permits varying the mass-dependent shape of the torque function, and S is an arbitrary factor multiplying the coupling coefficient K_{M1} , where K_{M1} would yield the correct P_{rot} at the solar age, if γ were zero. To keep dimensions correct, I absorbed a factor of $[f^2(0.65)]^{-\gamma}$ (corresponding to f^2 evaluated at the solar color) into S . Simultaneously adjusting the two parameters S and γ to maximize U_{M34} yields $S = 1.2$, $\gamma = 1.0$, with the joint K-S probability statistic $U_{M34} = 0.44$. This model gives the solar $P_{rot} = 26.7 \text{ d}$ at the solar age, slightly above the sidereal Carrington period of 25.4 d. This model is a good fit for all mass ranges; the K-S probabilities that simulated data and the model are drawn from the same distribution are $\{0.83, 0.97, 0.60, 0.70\}$ for the 4 color bands.

Performing similar fits for five well-studied clusters of various ages gives the results in the top five lines of Table 1. One can infer several systematic behaviors from this tabulation. The fit quality as shown by the joint K-S probability metric U_a is best for M34 (age 220 MYr), and is worse for both younger and older clusters. Indeed, for the youngest (Pleiades) and oldest (NGC 6811) clusters shown here the fits are poor, with only one or two of the color bands reporting a K-S probability U_{aj} better than 10%, and the other bands being

much worse. Also, both fitted parameters as well as the inferred solar P_{rot} at solar age show trends with cluster age. These changes are in the sense that, for increasing age, the I -sequence shape function of $(B - V)$ looks increasingly like a step function and less like a ramp, while the projected solar rotation periods tend to decrease with increasing cluster age. Recall that, motivated by the SEM, the MDM assumes that $P_{rot}(B - V, t)$ is the product of $t^{-1/2}$ and an age-invariant function $f(B - V)$, which in turn is related to the convective turnover time τ . Taken together, the fitting shortcomings just described suggest that none of these dependences are completely correct, though they happen to be roughly so for clusters similar in age to M34.

6.3. Comparison of 2ZM and SEM to MDM

With the methodology just described, it is straightforward to verify in a quantitative way that the 2ZM and SEM provide relatively poor matches to observed cluster data. To give a fair comparison with the MDM fits just described, I generalized the 2ZM and SEM torque laws so that each of them includes a scaling parameter S and a $(B - V)$ shape exponent γ . I varied the values of these parameters to give the best K-S probability, taken jointly over the same color bands as used in the previous section. The generalized torque laws I used were analogous to the one for the MDM. For the 2ZM:

$$\begin{aligned} \frac{dJ}{dt} &= SK_W \Omega^3 \left[\frac{R}{M^{1+\gamma}} \right]^{1/2}, & \Omega \leq \Omega_{crit}, \\ &= SK_W \Omega \Omega_{crit}^2 \left[\frac{R}{M^{1+\gamma}} \right]^{1/2}, & \Omega \geq \Omega_{crit}, \end{aligned} \quad (7)$$

And for the SEM:

$$\frac{dJ}{dt} = -SI_* \frac{\Omega^2}{2\pi} \left[\frac{2\pi k_I}{\tau^{1+\gamma}\Omega} + \frac{\tau^{1+\gamma}\Omega}{2\pi k_C} \right]^{-1}. \quad (8)$$

The cluster M34 is a good choice for comparing model cumulative distributions, because it is old enough that the C - and I -sequences are well separated, but young enough that a significant fraction of C -sequence stars remain. The 2ZM and SEM fitting results for this cluster are shown in the last two lines of Table 1. Figure 8 illustrates the cumulative probability distributions on which the K-S statistics are based, for two of the color bands used in the fits, for all (2ZM, SEM, MDM) best-fit models.

For the 2ZM, the U_{M34} statistic is fairly poor, though not as bad as for the worst clusters' (Pleiades, NGC 6811) fit with the MDM. But the shape exponent's fitted value of 5.5 is far different from the value suggested by theory (*i.e.*, roughly zero). Moreover, the K-S

probabilities for the individual color bands are fairly good (about 0.45) only for the two

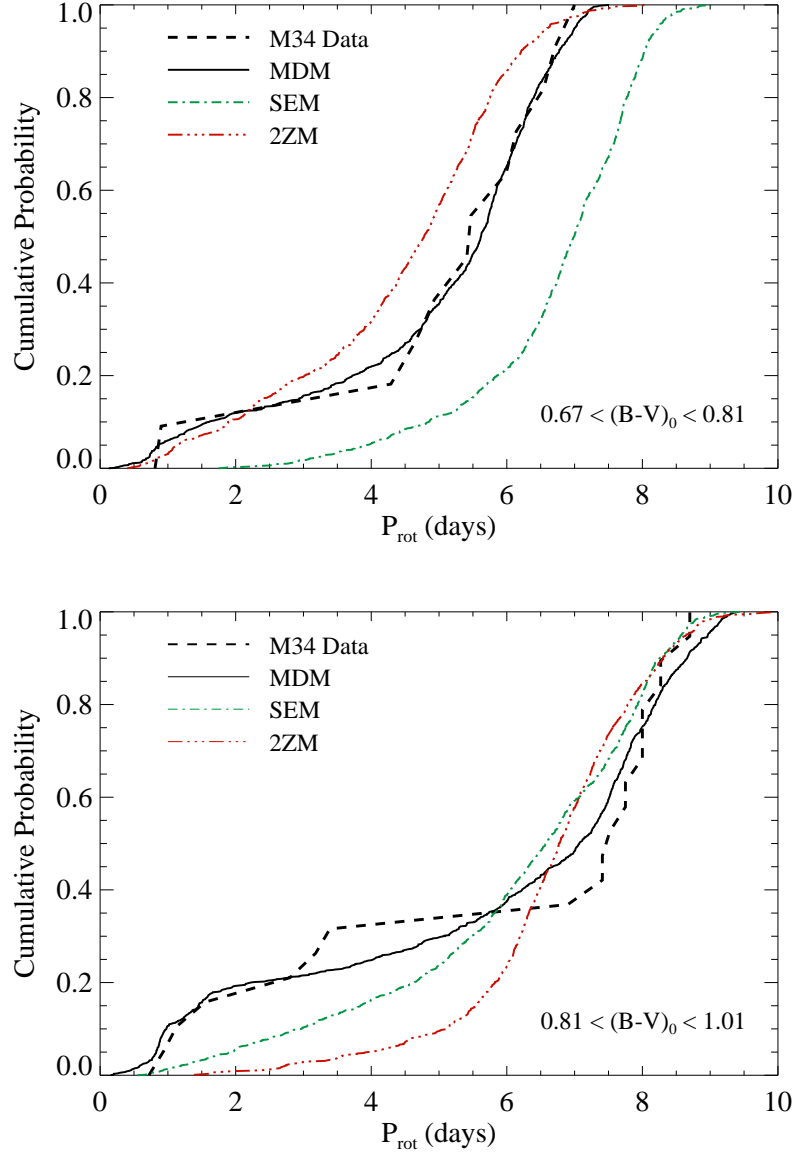


Fig. 8.— Cumulative probability estimates shown as functions of P_{rot} , for observations of the 220-MYr-old cluster M34, and for population synthesis runs based on the 2ZM, SEM, and MDM. The two panels show data summed over two different ranges of $(B - V)$ color, as marked. Observed periods are from Meibom et al. (2009); all modeling results are for best-fit model parameters as described in the text.

bluemoest colors, and are much worse (about .025) for the two redmoest colors. The U_{M34} statistic for the SEM is considerably worse than for the 2ZM, and indeed is worse than for any cluster fitted using the MDM. The SEM fit produces a K-S probability larger than 0.1 for only one of the color bands; all the rest are smaller than 0.002.

For both the 2ZM and the SEM, these fitting statistics suggest that one is attempting to force an inappropriate model onto the data, with results that may be locally acceptable, but that fail in a global sense. It is worth noting, however, that since most of the stars tabulated in the M34 data lie on the I -sequence, the fitting failures just described relate mostly to failures of the models to reproduce the $(B - V)$ variation of the I -sequence. Fig. 8 illustrates this; particularly in its upper panel, the SEM and 2ZM cumulative probability curves reveal failure to match the I -sequence through displacements to right or left of the data curve, for fairly long P_{rot} and for cumulative probabilities larger than about 0.3. But the shape of the I -sequence has only weak physical motivation for all of the models. So it seems likely that by choosing some other functional form for, say, the $f(B - V)$ function that appears in the SEM, one could achieve much better fits (although without necessarily adding substance to our physical understanding.)

At shorter periods and lower cumulative probabilities, Fig. 8 shows something more essential. In this part of the diagrams, the data curves have a step at periods around 2 days, and an adjacent spread of larger periods over which the curve’s slope is small. These features are the signature of the C -sequence stars at short periods and the paucity of stars at intermediate ones; the MDM reproduces both features fairly well, but the 2ZM and SEM do not.

7. Discussion

7.1. Summary of Conclusions

In the foregoing sections, I have described a modeling exercise in which I have tried to match observed P_{rot} -color diagrams using three different models of the stellar spindown process. In this attempt, I have assigned primary importance to the observed existence in fairly young clusters of two sequences of stars, first noted by Barnes (2003): the C -sequence at P_{rot} of about 2 days and less, separated by a poorly-populated gap from the I -sequence at longer periods.

The principal conclusion of the current modeling study is that previous models (the 2-zone model, or 2ZM *e.g.* Denissenkov et al. (2010), and Barnes symmetrical empirical model, or SEM (Barnes 2010; Barnes & Kim 2010)) do not adequately represent the best recent open

cluster observations. In particular, by virtue of the continuous way in which these models map initial conditions into the history of torque on a star, they are unable to produce C -sequences that are as populous, well-defined, or at periods as short as those seen in the observational data. I propose the so-called Metastable Dynamo Model (MDM) as a solution to this problem. Its key hypothesis is that some or all stars go through an early phase in which magnetic activity is present, but the angular momentum coupling to the stellar wind is very small. It appears to be quite difficult to explain the properties of the C -sequence without invoking some such mechanism that decouples many young stars from the stellar wind torque, at least for a time. Fits of the MDM parameters to cluster data constrain the strength of the angular momentum coupling for the hypothetical weakly-coupled stars to be at least 300 times less than for I -sequence stars. The typical lifetime for the weakly-coupled phase is found to be about 80 MYr for stars of $1 M_{\odot}$; the data are consistent with longer lifetimes of this phase for smaller-mass stars, but the form of this dependence is poorly constrained. All three model classes (2ZM, SEM, MDM) have failings, notably inability to reproduce the time history of the color dependence of P_{rot} on the I -sequence. For the MDM, these inaccuracies are smallest for the cluster M34 (age about 220 MYr), and are larger for both younger and older clusters.

7.2. Observational Tests

The foregoing analysis suggests a number of observational tests that may help choose among the various theories, test their premises, or refine their physical interpretations.

The 2ZM makes the striking prediction that most relatively young stars (ages between 50 and 300 Myr, depending on mass) on the I -sequence should have markedly different rotation rates in their CZs and in their radiative interiors. In principle, the radial variation of Ω can be measured with asteroseismology. This has been done for many years with solar pulsations, and indeed, using photometric data from the *Kepler* mission, recent analysis of pulsations in red giant stars has revealed large differences in rotation rate between the tiny degenerate core and the extensive convective envelope (Beck et al. 2012). Asteroseismic measurements of rotation in young Sun-like stars have not yet been successful, however. (Deheuvels et al. (2014) have measured rotational splitting in *Kepler* data for several subgiant stars. But since the method used requires detection of mixed oscillation modes, having properties of both pressure- and gravity-modes, it is not applicable to the relatively young stars under discussion here.) Young, magnetically active stars display larger photometric noise than do their older, inactive brethren, and moreover magnetic activity suppresses the surface amplitudes of acoustic oscillations, making them more difficult to observe (Chaplin et al. 2011).

This unfortunate combination has so far prevented conclusive asteroseismic measurements of radial differential rotation in Sun-like stars. Analysis of longer (full mission length) time series from *Kepler* may yet allow such measurements.

Apart from reproducing the morphology of the *C*- and *I*-sequences, a successful model of rotational evolution should also give the observed distribution of stars in the gap between sequences. For a uniform distribution of initial rotation periods, the MDM’s prediction in this respect is clear: Stars in the gap must have recently transitioned from weak- to strong-coupling modes, hence they are rapidly evolving to longer periods; as their periods increase, dP_{rot}/dt decreases. Thus the star density should be lowest at periods just above those in the *C*-sequence and rise towards longer periods, up to the *I*-sequence. This behavior is clearly visible in the probability density distributions shown in Fig. 7. Predictions for the 2ZM and the SEM are slightly more complicated, and little work has been done concerning them, but there are no fundamental obstacles to doing so. The observational picture is more difficult, however. Star counts between the *C*- and *I*-sequences are small, and as yet data are too sparse to make strong tests of the models within the period gap. Further observations are essential for this purpose.

Finally, if the MDM scenario is correct, then stars lying on the *C*-sequence must differ greatly from similar-mass stars in the period gap, having much weaker angular momentum coupling to the stellar wind. What could cause such a difference? Clearly there must be some difference in the wind, in the magnetic field that threads it, or both. Gross changes in the stellar wind seem implausible and in any case unobservable, given current techniques. If the difference is in the field, however, then diagnostics may be feasible. Observations of X-ray luminosity as a function of P_{rot} show no obvious step across the period range occupied by the *C*-sequence (Pizzolato et al. 2003). Therefore the hypothetical discontinuous change in coupling properties would likely be signalled not by a difference in the typical magnetic field strength, but rather by a change in its spatial organization. This idea is not new; it was suggested in Barnes (2003), and has since been explored using X-ray data by, e.g., Wright et al. (2011), by Gondoin (2012, 2013), with spectropolarimetry by Morin et al. (2011), and, in the context of ultra-cool dwarf stars, by combining X-ray and rotation data (Cook et al. 2013). A related line of argument starts with the observed Vaughan-Preston gap in the distribution of stars in P_{rot} - R'_{HK} space, where R'_{HK} is the Mt. Wilson Ca II activity index (Vaughan & Preston 1980). This gap was quickly interpreted as evidence for a small discrete set of dynamo classes, most clearly seen as relations between P_{rot} and the dynamo cycle period P_{cyc} (Durney et al. 1981; Brandenburg et al. 1998; Böhm-Vitense 2007). In the current context, perhaps the most intriguing result of these studies is the observation that some stars lie in a “supersaturated dynamo” state, described by Saar & Brandenburg (1999). Stars thus identified have short rotation and cycle periods, and the power-law relation be-

tween these periods has the opposite sign from that seen in stars with longer P_{rot} . Moreover, the transition between the supersaturated and other dynamo modes appears to be abrupt (because there are very few transitional objects seen), and involves a discontinuous change in the cycle period.

The various lines of study just described involve a wide range of stellar circumstances and several different (and hypothetical) formulations of dynamo physics. So it is not clear that all of these studies relate to the same phenomena, or are governed by the same processes. Nevertheless, taken together they reinforce the idea that a variety of dynamo modes might exist, yielding (among other properties) different partitioning of power across large and small spatial scales. If almost all of the magnetic energy were found in small-scale structures in which positive and negative field regions accurately cancel one another, then little field might penetrate to heights where the stellar wind expansion begins. The result would be an almost field-free wind, and only minimal torque on the star. Differences among photospheric spatial structures may be identifiable using Doppler imaging and spectropolarimetry, by comparing very rapid rotators against stars with similar activity diagnostics but slower rotation periods. Measuring the cycle periods of very fast rotators might also be revealing, as a probe of deeper-seated differences among the properties of stellar dynamos.

7.3. Final Considerations

It is worthwhile to reiterate a few points, and to raise some issues for further work. (1) The population synthesis calculations described above suggest that the MDM has some validity, but they are by no means conclusive evidence that it is correct, nor that the 2ZM or SEM are wrong. There may well be parameter choices for these latter models that will better reproduce the C -sequence population than the ones I have employed here. (2) Within the MDM framework, it appears that models enforcing solid-body rotation match the young-cluster observations, but there is as yet nothing to show that differentially-rotating models are excluded. (3) The basic MDM assumes that all stars begin life in the weakly-coupled dynamo mode. But in very young clusters there is evidence that the MDM's assumptions place too many stars on the C -sequence. Thus, perhaps only a fraction (perhaps as few as half) of all stars initially occupy the weak-coupling mode. A statistical test of this conjecture may be feasible with the data that are presently in hand. (4) All model classes have difficulty fitting the shapes of I -sequences with age, especially for stars older than a few hundred MYr. Indeed, given this difficulty, the Ω^3 torque law (hence the $t^{-1/2}$ period law) may be only an approximation. To do better may require a function of both Ω and mass; making a useful guess about the form of such a function will be difficult, lacking a physical picture of the

important processes.

I am grateful to Sydney Barnes and to Marc Pinsonneault for conversations that inspired and informed this work, and to Travis Metcalfe, David Soderblom, Soeren Meibom, and Lynne Hillenbrand for their useful comments on an early version of this paper.

REFERENCES

- Barnes, S. A. 2003, *ApJ*, 586, 464
- . 2010, *ApJ*, 722, 222
- Barnes, S. A., & Kim, Y.-C. 2010, *ApJ*, 721, 675
- Beck, P. G., Montalban, J., Kallinger, T., et al. 2012, *Nature*, 481, 55
- Belcher, J. W., & MacGregor, K. B. 1976, *ApJ*, 210, 498
- Böhm-Vitense, E. 2007, *ApJ*, 657, 486
- Brandenburg, A., Saar, S. H., & Turpin, C. R. 1998, *ApJ*, 498, L51
- Chaplin, W. J., Bedding, T. R., Bonanno, A., et al. 2011, *ApJ*, 732, L5
- Choi, P. I., & Herbst, W. 1996, *AJ*, 111, 283
- Cook, B. A., Williams, P. K. G., & Berger, E. 2013, *ArXiv e-prints*, arXiv:1310.6758
- Deheuvels, S., Doğan, G., Goupil, M. J., et al. 2014, *ArXiv e-prints*, arXiv:1401.3096
- Delorme, P., Collier Cameron, A., Hebb, L., et al. 2011, *MNRAS*, 413, 2218
- Denissenkov, P. A., Pinsonneault, M., Terndrup, D. M., & Newsham, G. 2010, *ApJ*, 716, 1269
- Durney, B. R., Mihalas, D., & Robinson, R. D. 1981, *PASP*, 93, 537
- Eaton, N. L., Herbst, W., & Hillenbrand, L. A. 1995, *AJ*, 110, 1735
- Epstein, C. R., & Pinsonneault, M. H. 2014, *ApJ*, 780, 159
- Gilman, P. A., Morrow, C. A., & Deluca, E. E. 1989, *ApJ*, 338, 528
- Gondoin, P. 2012, *A&A*, 546, A117
- . 2013, *A&A*, 556, A14
- Hartman, J. D., Bakos, G. Á., Kovács, G., & Noyes, R. W. 2010, *MNRAS*, 408, 475
- Hartman, J. D., Gaudi, B. S., Holman, M. J., et al. 2009, *ApJ*, 695, 336
- Irwin, J., & Bouvier, J. 2009, in *IAU Symposium*, Vol. 258, *IAU Symposium*, ed. E. E. Mamajek, D. R. Soderblom, & R. F. G. Wyse, 363–374

- Jackson, R. J., & Jeffries, R. D. 2012, MNRAS, 423, 2966
- Kawaler, S. D. 1988, ApJ, 333, 236
- Krishnamurthi, A., Pinsonneault, M. H., Barnes, S., & Sofia, S. 1997, ApJ, 480, 303
- MacGregor, K. B., & Brenner, M. 1991, ApJ, 376, 204
- Meibom, S., Mathieu, R. D., & Stassun, K. G. 2009, ApJ, 695, 679
- Meibom, S., Mathieu, R. D., Stassun, K. G., Liebesny, P., & Saar, S. H. 2011a, ApJ, 733, 115
- Meibom, S., Barnes, S. A., Latham, D. W., et al. 2011b, ApJ, 733, L9
- Mermilliod, J.-C. 1995, in *Astrophysics and Space Science Library*, Vol. 203, *Information & On-Line Data in Astronomy*, ed. D. Egret & M. A. Albrecht, 127–138
- Mestel, L. 1968, MNRAS, 138, 359
- Morin, J., Dormy, E., Schrunner, M., & Donati, J.-F. 2011, MNRAS, 418, L133
- Palla, F., & Stahler, S. W. 1990, ApJ, 360, L47
- Paxton, B., Bildsten, L., Dotter, A., et al. 2011, ApJS, 192, 3
- Pinsonneault, M. H., Kawaler, S. D., & Demarque, P. 1990, ApJS, 74, 501
- Pizzolato, N., Maggio, A., Micela, G., Sciortino, S., & Ventura, P. 2003, A&A, 397, 147
- Press, W. H., Flannery, B. P., Teukolsky, S. A., & Vetterling, W. T. 1989, *Numerical recipes in C. The art of scientific computing*
- Rebull, L. M. 2001, AJ, 121, 1676
- Rebull, L. M., Wolff, S. C., & Strom, S. E. 2004, AJ, 127, 1029
- Saar, S. H., & Brandenburg, A. 1999, ApJ, 524, 295
- Skumanich, A. 1972, ApJ, 171, 565
- Stauffer, J. R., Caillault, J.-P., Gagne, M., Prosser, C. F., & Hartmann, L. W. 1994, ApJS, 91, 625
- Tomczyk, S., Schou, J., & Thompson, M. J. 1995, ApJ, 448, L57

Vaughan, A. H., & Preston, G. W. 1980, PASP, 92, 385

Walker, M. F. 1990, PASP, 102, 726

Weber, E. J., & Davis, Jr., L. 1967, ApJ, 148, 217

Wright, N. J., Drake, J. J., Mamajek, E. E., & Henry, G. W. 2011, ApJ, 743, 48

Table 1: Results of K-S Fits to Cluster P_{rot} Data

Cluster	Age	Nstars	Model	Scale	Exponent	FOM
	(MYr)		Class	S	γ	U_a
Pleiades	125	147	MDM	1.37	1.50	-5.15
M35	150	172	MDM	1.36	0.75	-2.22
M34	220	70	MDM	1.20	1.00	-0.44
M37	550	187	MDM	0.84	0.45	-3.60
NGC 6811	1000	48	MDM	0.88	-0.46	-7.52
M34	220	70	2ZM	1.21	5.50	-3.68
M34	220	70	SEM	1.60	0.10	-9.54

Note. — The sources for P_{rot} data for the various clusters are (Pleiades: Hartman et al. (2010)), (M35: Meibom et al. (2009)), (M34: Meibom et al. (2011a)), (M37: Hartman et al. (2009)), (NGC 6811: Meibom et al. (2011b)).